OPTICAL REVIEW Vol. 7, No. 5 (2000) 442–447

Optical Coherence Tomography System based on Synthesis of Optical Coherence Function with a Wavelength-Scanning Laser Source

Hajime HIRATSUKA,[1,2] Kentaro MORISAKI[2] and Takeaki YOSHIMURA[2,*]

[1]*Advanced Technology Laboratory, KUBOTA Corporation, 1-1, Hama, Amagasaki, Hyogo, 661-8567 Japan,* [2]*Faculty of Engineering, Kobe University, 1-1, Rokkodai, Nada, Kobe, 657-8501 Japan*

(Received May 15, 2000; Accepted June 30, 2000)

A new optical coherence tomography system using a wavelength-scanning laser source is presented. The system has the advantage that the depth resolution can be controlled by the scanning range. In general, rapid scanning of the wavelength varies the output power of the laser source, and it is difficult to detect a weak signal of reflected light from the scattering object. By synchronizing the intensity-integrated detector with the variation, the dynamic range of the detection has been improved. To confirm the performance, tomographic imaging of biological tissues is demonstrated.

Key words: optical coherence tomograpy, coherence function, wavelength-scanning, synchronizing, dynamic range, biological tissue

1. Introduction

Non-invasive techniques like X-ray computed tomography, magnetic resonance imaging or positron emission tomography have been developed, each of which has different advantages and limitations in clinical applications. In modern medicine diagnosis during a regular medical checkup to identify a disease in an early stage has become more important than the expensive treatment of an advanced illness. In recent years several so-called optical coherence tomography (OCT) methods have been investigated for imaging inner structures of biomedical tissues, based on the probe light being safe for living tissues in comparison with ionizing radiation such as X-rays and γ-rays. The OCT techniques detect a reflectance in the tissues from the intensity of reflected ballistic light. However, there are difficulties since a high dynamic range is required to detect the ballistic light because many biomedical tissues act highly scattering and the light intensity is usually weak even if near-infrared light is used.

There are two techniques to extract the depth information together with the reflectance: optical frequency domain reflectometry (OFDR)[1–8] and optical coherence domain reflectometry (OCDR).[9–18] Both are based on an interferometry that yields a high depth resolution. OFDR uses a narrow band source swept continuously over a wide optical frequency and the optical path difference in the interferometer is addressed in beat frequencies of the interference intensity. The power spectrum of the beat signal thus provides the reflectance distribution along the depth direction in the object. The depth resolution is inversely proportional to the sweeping range. In this method of sweeping the optical frequency, however, it is difficult to obtain high depth resolution because of mode-hopping and power variation of the laser source. OCDR extracts the depth information, whose position is balanced with the reference arm length in the interferometer, by utilizing a coherence gate of a broad bandwidth source such as superluminescent diodes or femtosecond pulse lasers. For example, femtosecond pulse laser technology has the depth resolution of one micrometer.[12] This resolution cannot be controlled, however, because the gate-width of the coherence function is determined by the bandwidth of the light source.

In tomographic imaging it is important that the depth resolution can be adjusted to detect weak ballistic light with high efficiency. Synthesis of the optical coherence function makes it possible to control the depth resolution. Several methods of synthesizing this function have been proposed[15–18]; in this study, we use high-speed and linear wavelength-scanning of the laser source. In the scanning method the most serious problem is the power variation of the light source. To overcome this, a new OCT system synchronizing the integration detector of intensity with a wavelength-scanner is presented, and tomographic imaging for biological tissue is then realized.

2. Principle of OCT Imaging

To extract the reflectance information at a certain depth in an object, most OCT systems utilize a Michelson interferometer as shown in Fig. 1. The light is divided into two beams by a beam splitter, and illuminates simultaneously both a reference mirror and an object. The reference beam is reflected by the reference mirror, and the object beam is reflected by a plane of an amplitude reflectance $r_s(z+\Delta z)$ at the depth $z+\Delta z$ from the object surface. Here, z is the position balanced with the reference mirror and Δz is the deviation from the balanced position. These two reflected beams are superposed on the beam splitter and detected at the observation plane. The object beam has a time delay $\tau=2\Delta z/c$ in comparison with the reference beam, where c is the light speed. The intensity on the observation plane is given by

*E-mail: csyoshi@kobe-u.ac.jp

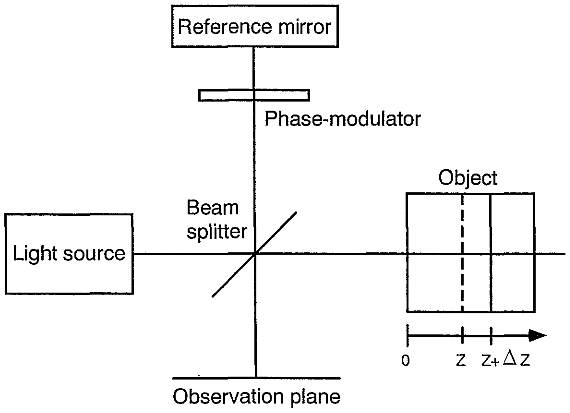

Fig. 1. Schematic diagram of OCT system.

$$I(\tau)=I_o+2r_s(z+\Delta z)|\Gamma(\tau)|\cos(2\pi f\tau-\phi_r), \qquad (1)$$

where f is the optical frequency, $|\Gamma(\tau)|$ is the coherence function, I_o is the dc term independent of τ and ϕ_r is the initial phase of the reference beam. The interference term contains information on reflectance distribution $r_s(z)$. If the reflectance $r_s(z)$ is distributed along the depth direction, the equation is transformed by a convolution integral of the reflectance function with the coherence function. Therefore, the coherence function $|\Gamma(\tau)|$ acts as a window function for the distribution $r_s(z)$.

As a light source, let us use a wavelength-scanning laser source, whose scanning speed is sufficiently rapid. We assume that average power within the response time of the detector to be used has a rectangular spectrum as

$$S(f)=\mathrm{rect}\left(\frac{f-f_c}{\Delta f}\right), \qquad (2)$$

where f_c and Δf are the center frequency and the bandwidth of the scanning, respectively. By Wiener-Khinchine's theorem, the normalized coherence function is given by

$$\frac{|\Gamma(\tau)|}{I_o}=|\mathrm{sinc}(\Delta f\tau)|. \qquad (3)$$

As seen from Fig. 2, the coherence length is

$$c\tau_c=\frac{c}{\Delta f}, \qquad (4)$$

where τ_c is the coherence time. The coherence length can be controlled by synthesizing many laser beams of different wavelengths. The laser source whose wavelength is scanned over a wide bandwidth has a short coherence length and its coherence function becomes a delta-function-like shape whose center is $\tau=0$ or $\Delta z=0$. Therefore, interference intensity gives the reflectance on the plane of the depth z.

Now let the reference beam be phase-modulated in time. Since the initial phase is time-varying as $\phi_r(t)$, the interference intensity is also rewritten by a time-dependent function as

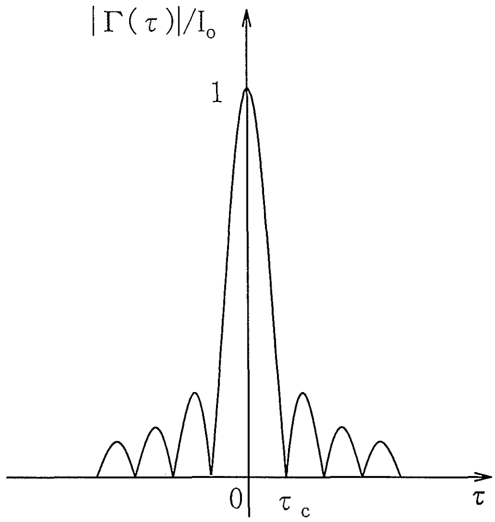

Fig. 2. Coherence function of rectangular spectrum.

$$I(t)=I_o+2r_s(z)|\Gamma(\tau)|\cos[2\pi f_c\tau-\phi_r(t)]. \qquad (5)$$

The reflectance information is contained within the amplitude of temporally fluctuating intensity. The amplitude can be evaluated by the variance or the 2nd order moment. When $\phi_r(t)$ is linearly modulated in time, the time-averaged moment M is

$$M=\frac{\langle (I(t)-I_o)^2\rangle}{I_o^2}=2\frac{|\Gamma(\tau)|^2}{I_o^2}R_s(z), \qquad (6)$$

where $\langle\quad\rangle$ means the time-averaging and $R_s(z)=r_s(z)^2$ is the reflectance at a position z. The moment provides the reflectance $R_s(z)$ at a depth z in the object. If either the reference mirror or the object is scanned along the optical axis, the reflectance distribution along the depth direction of the object can be obtained.

3. OCT System with a Wavelength-Scanning Laser Source

3.1 Experimental Setup

The OCT imaging system which consists of an optical system of a Michelson interferometer and a detection system of the moment processing has been prepared as schematically shown in Fig. 3. The light is divided into two waves whose intensity ratio is adjusted by a 1/2-wave plate and a polarizing beam splitter. The object- and the reference-waves are superposed on a polarizing beam splitter, and passed through the spatial filter of the two-lens imaging system with a pinhole. The superposed light is detected by a CCD camera (Hamamatsu Photonics; Model C4880-80, 14 bit). The object is mounted on a pulse-motor-driven stage which moves along the optical axis with a resolution of 0.5 μm/pulse. The depth to be measured is selected by the stage.

The reference mirror is mounted on a piezoelectric transducer (PZT). The applied voltage to the PZT is a triangular waveform whose amplitude gives the phase-

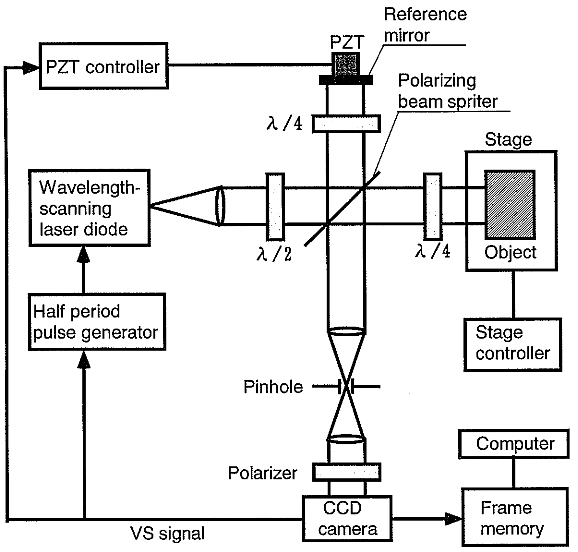

Fig. 3. OCT imaging system with the optical system of Michelson interferometer and the data processing system due to the moment method.

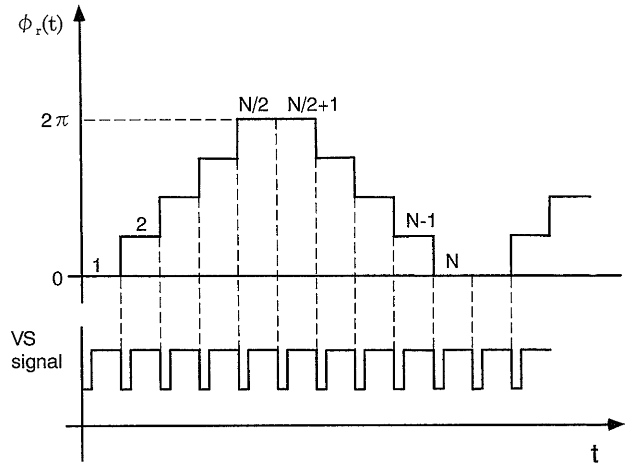

Fig. 4. Phase modulation synchronized with VS signal.

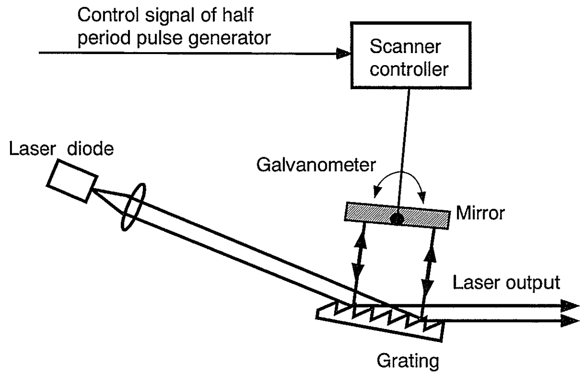

Fig. 5. Arrangement of wavelength scanning laser diode.

change of 2π. The phase-modulation is done step by step as shown in Fig. 4. By synchronizing the applied voltage with the vertical synchronizing signal (VS signal) of the CCD camera, the modulated phase is kept at a constant value during a frame time. The video signal from the CCD camera is stored as 14bit quantization signals over N frames. Here the frame number N is an even number. Let us define $I(t_i)=I_i$ to the signal of the i-th frame for a certain pixel. The 2nd order moment is calculated by

$$M=\frac{\frac{1}{N}\sum_{i=1}^{N}(I_i-I_{\rm ave})^2}{I_{\rm ave}{}^2} \tag{7}$$

where

$$I_{\rm ave}=\frac{1}{N}\sum_{i=1}^{N}I_i. \tag{8}$$

If a large number is selected as N, the averaging is sufficient.

3.2 Synthesis of the Optical Coherence

The laser light source (Environmental Optical Sensors; Model 2001-ECU) has been developed for rapid scanning of laser oscillation frequency. As shown in Fig. 5, the light source consists of a laser diode, a grating and a mirror mounted upon a galvanometer (Cambridge Technology; Model 6450). The wavelength of laser light is controlled by the rotation-angle of the mirror. The mirror is rotated to right and left by the galvanometer, the period of which is synchronized by the control signal generated by the half period pulse generator. The relation among the VS signal, the control signal of the pulse generator, applied voltage to the galvanometer and the output power is shown in Fig. 6. It is found that, although the VS signal of the present CCD camera can be varied from an interval of 2.0 s to 20.0 ms, the mirror responds with a sufficient speed. On the other hand, the laser power is varied because the wavelength is scanned widely beyond a gain range of laser oscillation. If the periodic variation of the power is synchronized with the control signal (or the VS signal), however, the variation is removed by the time-integrated intensity during a frame time. The power spectrum detected by the CCD camera is shown in Fig. 7. The response time of the camera is equal to the frame time and the coherence function is accurately synthesized by synchronous detection of the integrated intensity. The depth resolution depends on the bandwidth of the light source. As seen in the figure, the bandwidth is $\Delta\lambda=37$ nm, or $\Delta f=16.5$ THz, so the depth resolution of the system is very high. The wavelength-scanning laser source has a peak gain near the center wavelength of 820 nm, while the output power becomes lower at 801 and 837 nm away from the wavelength. The variation of intensity suppresses the sidelobes of coherence function.

4. Measurements of Physical Objects

4.1 Performance of the Synthesized Light Source

The performance of the present system is made evident by measuring a single reflection plate. The plate has

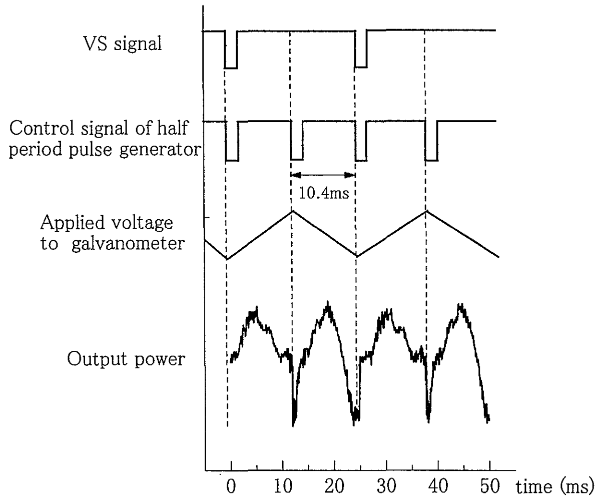

Fig. 6. Relation among the VS signal, the control signal of half period pulse generator, applied voltage to galvanometer and output power.

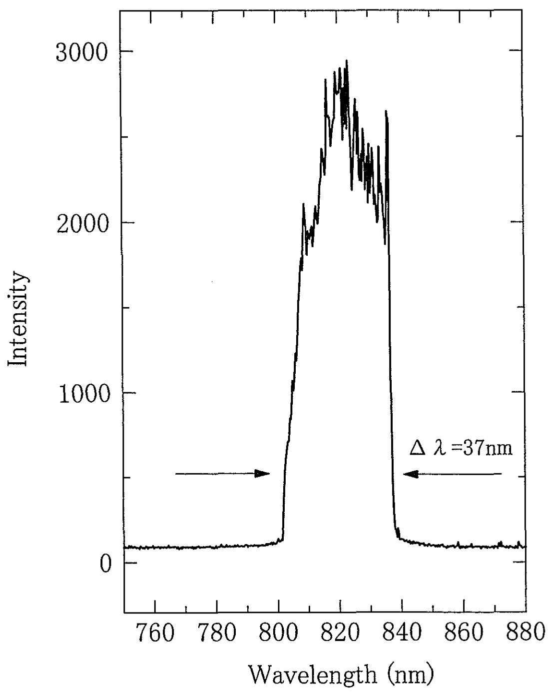

Fig. 7. Power spectrum of the light source whose wavelength is scanned in a frame time.

been moved along the optical axis by the deviation Δz from the position z balanced with the reference arm length in the interferometer. The normalized moment (or variance) of integrated intensity at a certain pixel is shown in Fig. 8, which represents the squared coherence function as seen from Eq. (6). The full width of the half maximum (FWHM) of the coherence function corresponds to 10 μm. It is found that the synthesized coherence function is sharp so that the depth resolution of the present OCT system is sufficiently high. If the voltage ap-

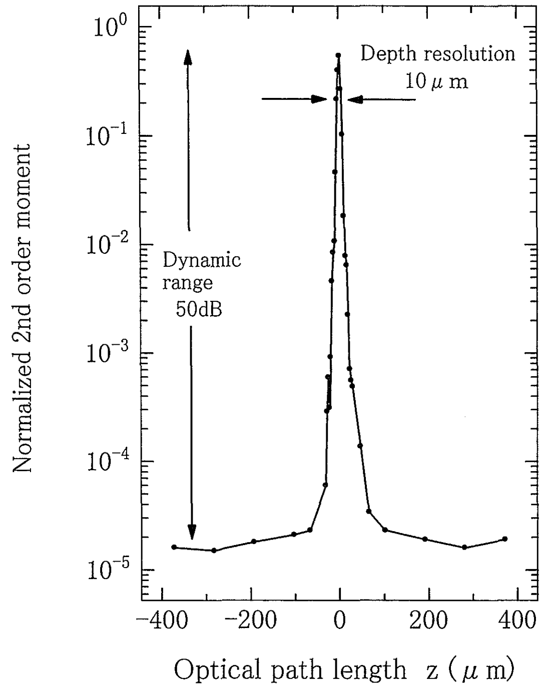

Fig. 8. 2nd order moment for a single reflection plate at a certain pixel.

plied to the galvanometer is set to a lower amplitude, the scanning range of wavelength becomes narrower with decrease of the amplitude, and as a result the depth resolution becomes wider than 10 μm. That is, use of the synthesized light source provides the advantage that the depth resolution can be electrically controlled.

To enlarge a measurable depth range in a scattering medium requires a wide dynamic range for detection of the reflected interference intensity. As seen from Fig. 8, the background level of the empty region is the order of 10^{-5}, which gives the dynamic range of 50 dB in the system. The level is the result of both the power fluctuation of the laser source and the sidelobes of the coherence function. The rapid wavelength-scanning of the laser source causes obstructive periodic variations of the output power. The variance (moment value) due to data-processing used in the present system is also equivalent to the variation strength itself. Therefore, the obstructive variation of the power yields an undesirable increase of background levels. By synchronizing both the scanning and the phase-modulation of the reference light with intensity-integration in the CCD camera, however, the undesirable variation of the interference intensity is sufficiently removed. The sidelobe level of the other factor depends on the spectral shape of synthesized light. For a rectangular spectrum, the sidelobe level is of the order of 10^{-4}. As seen in Fig. 7, the spectrum is fortunately given by a smooth function, so that it suppresses the sidelobe level to one order lower. The dynamic range has been improved by working the scanning system and the phase-modulation system with the VS signal of the

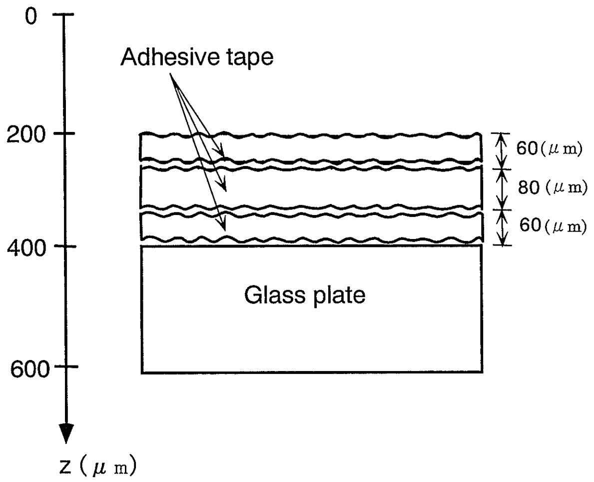

Fig. 9. Structure of the test sample.

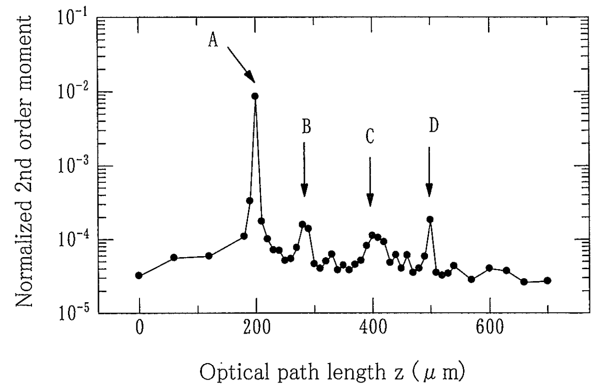

Fig. 10. 2nd order moment along z-axis for the test sample.

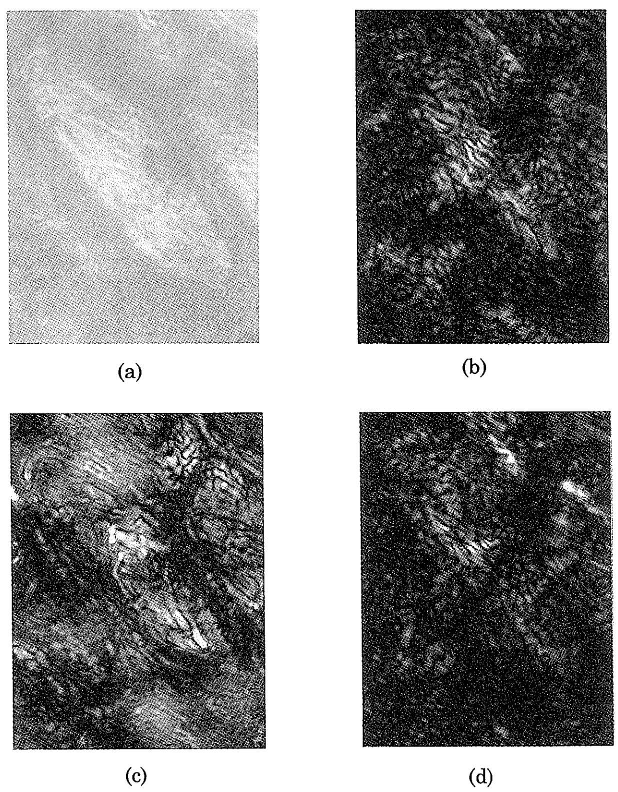

Fig. 11. Tomographic images of onion cells: (a) Normal microscope-image of the onion cells, (b) Upper surface of onion cells, (c) Cross section of 150 μm below the surface, (d) Bottom surface of one onion cell located 300 μm below the upper surface.

CCD camera.

4.2 Reflectance Imaging through Scattering Media

To confirm the possibility of reflectance measurements through scattering media, the test sample of a multi-layer object has been examined. The sample consists of three sheets of adhesive tape closely superposed on a glass plate as shown in Fig. 9. The three sheets are 60, 80 and 60 μm thick and both sides of each sheet are rough surfaces. When mean output power of the laser source is about 25 mW, the normalized moment of the interference intensity at a certain pixel is shown in Fig. 10. These peaks A, B, C and D show boundaries between the air and the first sheet, between the first and the second sheet, between the second and the third sheet and between the third sheet and the glass plate, respectively. Since the refractive index of the sheet is $n=1.5$ in the present wavelength region, the distance between the peaks corresponds to the optical path length 90, 120 and 90 μm. The peak-height decreases as the position of boundaries deepens from the object surface. This means that the incident light diffuses and/or reflects at each boundary. The last peak D is higher than peak C because a normal reflection light due to the smooth surface of the glass plate is included in addition to the reflected light scattered by the rough surface of the sheet.

The present system is available for imaging a cross section in xy-plane perpendicular to a depth direction both by using the CCD camera of an area sensor and by processing experimental data at each pixel independently. Furthermore, the focusing condition of the cross section on the observation plane is always satisfied by positioning the object with the stage. To investigate the performance of the imaging system, tomographic imagings at different depths in onion cells were measured as shown in Fig. 11. Here, the sizes of all images are 150 × 200 μm (300 × 400 pixel), the frame time of the CCD camera is 0.812 s and the number of frames is $N=128$. So, the data required for each image have been stored in frame memories within a measuring time 104 s. The figure(a) shows the normal microscope-image of the onion cells obtained only by the object light. The figures (b),(c) and (d) show the upper surface of the onion cells, the cross section of 150 μm below the surface, and the bottom surface of one onion cell located 300 μm below the upper surface, respectively. As seen from the figure (c), the structure of inner cell and the cell wall are clearly imaged. Thus, two-dimensional tomographic imaging of a depth chosen arbitrarily is possible.

5. Conclusions

A new OCT system based on synthesis of the coherence function using a wavelength-scanning laser source has been presented. The system can control its depth resolution, because the broadness of the synthesized coherence function can be arbitrarily selected by changing the wavelength-scanning range. The power variation caused by the wavelength-scanning has been suppressed by synchronously combining the intensity-integration in the CCD camera with the periodic variation of the power. Consequently, the dynamic range of the moment detection has been improved. Finally, two-dimensional tomographic imaging of reflectance in onion cells as the scattering medium has been realized by the CCD camera.

Acknowledgment

Development of the scanning laser source was technically supported by Electronics Optics Research, Ltd.

References

1) A. F. Fercher, C. K. Hitgenberger, G. Kamp and S. Y. El-Zaiat: Opt. Commun. **117** (1995) 43.
2) F. Lexer, C. K. Hitgenberger, A. F. Fercher and M. Kulhavy: Appl. Opt. **36** (1997) 6548.
3) L. Rovati, U. Minoni and F. Doccho: Opt. Lett. **22** (1997) 850.
4) T. Yoshimura, N. Masazumi and Y. Shigematsu: Opt. Rev. **4** (1997) 221.
5) T. Yoshimura, H. Hiratsuka, E. Kido and K. Yamada: Proc. SPIE **3479** (1998) 207.
6) H. Hiratsuka, E. Kido and T. Yoshimura: Opt. Lett. **23** (1998) 1420.
7) C. K. Hitzenberger, M. Kulhavy, F. Lexer, A. Baumgartner and A. F. Fercher: Proc. SPIE **3251** (1998) 47.
8) D. Holscher, U. Haberland, D. Pieknick and V. Blazek: Proc. SPIE **3251** (1998) 68.
9) D. Huang, E. A. Swanson, C. P. Lin, J. S. Schuman, W. G. Stinson, W. Chang, M. R. Hee, T. Flotte, K. Gregory, C. A. Puliafito and J. G. Fujimoto: Science **254** (1991) 1178.
10) M. J. Yadlowsky, J. M. Schmitt and R. F. Bonner: Appl. Opt. **34** (1995) 5699.
11) W. Drexler, U. Morgner, F. X. Kartner, C. Pitris, S. A. Boppert, X. D. Li, E. P. Ippen and J. G. Fujimoto: Opt. Lett. **24** (1999) 1221.
12) T. Yoshimura, K. Kida and N. Masazumi: Opt. Commun. **117** (1995) 117.
13) A. GH. Podoleanue, G. H. Dobre, D. J. Webb and D. A. Jackson: Opt. Lett. **22** (1997) 1039.
14) E. Beaurepaire, A. C. Boccara, M. Lebec, L. Blanchot and H. S. Jalmec: Opt. Lett. **23** (1998) 244.
15) Y. J. Rao, Y. N. Ning and D. A. Jacson: Opt. Lett. **18** (1993) 462.
16) K. Hotate and T. Okugawa: Opt. Lett. **17** (1992) 1529.
17) K. Hotate: J. Lightwave Technol. **12** (1994) 1247.
18) Z. He and K. Hotate: Opt. Lett. **24** (1999) 1502.